Clim Dyn
DOI 10.1007/s00382-013-1749-1

Future surface mass balance of the Antarctic ice sheet and its influence on sea level change, simulated by a regional atmospheric climate model

S. R. M. Ligtenberg · W. J. van de Berg · M. R. van den Broeke · J. G. L. Rae · E. van Meijgaard

Received: 1 May 2012 / Accepted: 22 March 2013

Abstract A regional atmospheric climate model with multi-layer snow module (RACMO2) is forced at the lateral boundaries by global climate model (GCM) data to assess the future climate and surface mass balance (SMB) of the Antarctic ice sheet (AIS). Two different GCMs (ECHAM5 until 2100 and HadCM3 until 2200) and two different emission scenarios (A1B and E1) are used as forcing to capture a realistic range in future climate states. Simulated ice sheet averaged 2 m air temperature (T_{2m}) increases (1.8–3.0 K in 2100 and 2.4–5.3 K in 2200), simultaneously and with the same magnitude as GCM simulated T_{2m}. The SMB and its components increase in magnitude, as they are directly influenced by the temperature increase. Changes in atmospheric circulation around Antarctica play a minor role in future SMB changes. During the next two centuries, the projected increase in liquid water flux from rainfall and snowmelt, together 60–200 Gt year^{-1}, will mostly refreeze in the snow pack, so runoff remains small (10–40 Gt year^{-1}). Sublimation increases by 25–50 %, but remains an order of magnitude smaller than snowfall. The increase in snowfall mainly determines future changes in SMB on the AIS: 6–16 % in 2100 and 8–25 % in 2200. Without any ice dynamical response, this would result in an eustatic sea level drop of 20–43 mm in 2100 and 73–163 mm in 2200, compared to the twentieth century. Averaged over the AIS, a strong relation between ΔSMB and ΔT_{2m} of 98 ± 5 Gt w.e. year^{-1} K^{-1} is found.

Keywords Antarctica · Future surface mass balance · Sea level rise

1 Introduction

The fourth Assessment Report of the Intergovernmental Panel on Climate Change (IPCC AR4) projects global sea level to rise by 0.18–0.59 m at the end of the twenty first century, relative to the end of the twentieth century, excluding ice dynamical effects (IPCC 2007). Currently (1993–2009), the rate of global sea level rise (SLR) is $\sim$3.3 mm year^{-1} (Nicholls and Cazenave 2010). The largest contributors to SLR are the melting of ice sheets, ice caps and valley glaciers and thermal expansion of ocean water (Church et al. 2011). The two major ice sheets of Greenland and Antarctica lost mass at a combined rate of 402 ± 201 Gt year^{-1} (1.1 ± 0.6 mm SLR year^{-1}) over the 2003–2008 period (Van den Broeke et al. 2011), hence contributing $\sim$30 % to ongoing SLR. In a warmer future climate, the relative contribution of these ice sheets to SLR is expected to increase further (Rignot et al. 2011).

Because of its size and remoteness, estimating the Antarctic ice sheet (AIS) mass balance and thereby its contribution to SLR is difficult. Three methods are

S. R. M. Ligtenberg (✉) · W. J. van de Berg · M. R. van den Broeke
IMAU, Universiteit Utrecht, Utrecht, The Netherlands
e-mail: S.R.M.Ligtenberg@uu.nl

W. J. van de Berg
e-mail: W.J.vandeBerg@uu.nl

M. R. van den Broeke
e-mail: M.R.vandenBroeke@uu.nl

J. G. L. Rae
Met Office, Hadley Centre, Exeter, UK
e-mail: jamie.rae@metoffice.gov.uk

E. van Meijgaard
KNMI, De Bilt, The Netherlands
e-mail: vanmeijg@knmi.nl

Published online: 16 April 2013

currently used: (i) the volumetric method, (ii) the gravimetry method and (iii) the mass budget method. The first converts remotely sensed surface elevation changes into mass changes (Davis et al. 2005), the second deduces mass changes in time directly from satellite measured gravity changes (Velicogna 2009) and the third differences mass in- and output, i.e. surface mass balance (SMB) and ice discharge (Rignot et al. 2011). Over the last 30–50 years, the SMB of the AIS showed little change (Monaghan et al. 2008; Lenaerts et al. 2012a). Combined with an increase in ice discharge, this currently leads to a positive contribution of the AIS to SLR: 0.2 ± 0.15 mm year^{-1} (Sheperd et al. 2012). Volumetric and/or gravimetric measurements suggest zero mass balance to a small mass gain in East Antarctica, and significant mass losses in West Antarctica and the Antarctic Peninsula (Davis et al. 2005; Pritchard et al. 2009; Velicogna 2009). The first and second method are fully based on observations and can therefore not be used to predict the future mass balance of Antarctica. For the third method however, future SMB and ice dynamics can be estimated with the use of climate and ice dynamical models.

The AIS is the largest reservoir of frozen fresh water on Earth; if melted completely, global sea level would rise by about 57 m (Lythe et al. 2001). With a mass turnover of $\sim$2,500 Gt year^{-1} (Lenaerts et al. 2012a), equivalent to $\sim$6.9 mm eustatic sea level change, even a relatively minor change (<10 %) in the AIS mass balance has a significant effect on global sea level. With temperatures rising globally, the Antarctic climate is also expected to warm, probably resulting in more melting in low-lying regions, and more snowfall continent-wide because of the increased water vapor holding capacity of the Antarctic atmosphere (Krinner et al. 2007). The mass gain from enhanced snowfall is expected to be larger than the mass loss from enhanced runoff. Previous studies indicate that increasing temperatures cause a 5–9 % K^{-1} mass input increase of the AIS (Wild et al. 2003; Gregory and Huybrechts 2006; IPCC 2007). For the coming century, the SMB of the AIS is therefore expected to cause a sea level drop of $\sim$50 mm (Krinner et al. 2007; Bengtsson et al. 2011). On the other hand, changes in ocean circulation may have the potential to enhance melt rates at the bottom of ice shelves by directing warmer water underneath them (Hellmer et al. 2012). This could lead to thinning of these ice shelves from below and thereby reducing the buttressing effect on outlet glaciers, and increasing ice discharge (Rignot and Jacobs 2002; Pritchard et al. 2012). How this will contribute to sea level change in the twenty first century is currently uncertain.

Here, we present estimates of the future SMB of the AIS and its impact on SLR, as simulated by a regional atmospheric climate model. The horizontal model resolution of coupled atmosphere–ocean global climate models (GCMs) is currently insufficient to accurately resolve changes in the Antarctic coastal climate and SMB processes are often poorly parameterized in these models. Moreover, an accurate treatment of SMB requires a detailed description of processes in the snowpack. The regional atmospheric climate model RACMO2 has a higher resolution and includes a specially-developed multi-layer snow model (Ettema et al. 2009; Kuipers Munneke et al. 2011). In this study, RACMO2 is forced at the boundaries by two different GCMs, each driven by two different greenhouse gas emission scenarios (A1B and E1), to obtain a range of possible future SMB scenarios. To check the reliability of the forcing fields, simulations for the period 1980–1999 are compared to a RACMO2 benchmark simulation forced by re-analysis data. Modelling of future ice-dynamics, to make an estimate of the AIS future mass balance, is outside the scope of this paper. In Sect. 2 of this paper, RACMO2, the GCMs and the emission scenarios are discussed. In Sect. 3, we present a comparison of the GCM and re-analysis forced simulations for the 1980–1999 climate. Thereafter, the results of the future scenarios are discussed in Sect. 4, followed by conclusions and discussions in Sect. 5.

2 Methods

2.1 Surface mass balance

The surface mass balance (SMB) of an ice sheet is defined as the annual sum (in Gt year^{-1}) of precipitation (P), surface sublimation (SU_s), runoff (RU), erosion by drifting snow (ER_{ds}) and sublimation due to drifting snow (SU_{ds}):

$$\mathrm{SMB} = \int_{year} (\mathrm{P} - \mathrm{SU_s} - \mathrm{RU} - \mathrm{ER_{ds}} - \mathrm{SU_{ds}})\mathrm{d}t \qquad (1)$$

In Antarctica, runoff is currently small because nearly all liquid water from snowmelt and rainfall refreezes in the firn layer. Sublimation of surface and drifting snow is the most important ablation term for the AIS, yet it is an order of magnitude smaller than accumulation by snowfall. Erosion by blowing snow is small on a continental scale and only locally important. Therefore, the current SMB of the AIS and its temporal and spatial variability is mainly determined by snowfall (Lenaerts and Van den Broeke 2012).

2.2 Regional atmospheric climate model RACMO2

All simulations are performed with the regional atmospheric climate model RACMO2 (Van Meijgaard et al. 2008). At the lateral boundaries of the domain, RACMO2

is forced using fields of temperature, specific humidity, zonal and meridional wind components, and surface pressure from either GCM or re-analysis output. Relaxation of RACMO2 prognostic variables towards external forcings is restricted to the boundary relaxation zone (Fig. 1). External forcings are updated every six hours and linearly interpolated in time to yield accurate values in between. Sea surface temperatures and sea-ice extent are also prescribed from the forcing model. The version of RACMO2 used for this study includes a snow model that calculates temperature, density and meltwater processes (percolation, retention, refreezing and runoff) in the snow (Ettema et al. 2009), and an improved albedo scheme, where the snow albedo depends on snow grain size (Kuipers Munneke et al. 2011). For this study, contributions from drifting snow processes have not been included, because the module of Lenaerts and Van den Broeke (2012) was not yet fully implemented when we started the simulations.

For contemporary climate studies of the AIS (1–30 years), RACMO2 has been run on grids with 27 and 5.5 km horizontal resolution (Lenaerts et al. 2012a, b). However, for the number of simulation years considered here (660 years in total), a horizontal resolution of 55 km is considered a good trade-off between computational expense and spatial detail; doubling the grid resolution would multiply the computational time by a factor 10. Moreover, the annual integrated SMB of the AIS at 55 km resolution (Van de Berg et al. 2006) is similar to that at 27 km resolution (Lenaerts et al. 2012a). For the scenario runs, the largest uncertainty therefore derives not from the model resolution but from the chosen forcing model and scenario. Given this information, and the fact that a 27 km resolution run is ten times as expensive as a 27 km run, we chose 55 km as final resolution. The model topography, grid resolution and lateral relaxation boundary of the domain are shown in Fig. 1.

For the period 1980–1999, a RACMO2 reference simulation, forced by ERA-40 re-analysis data from the European Centre for Medium-Range Weather Forecasts (Uppala et al. 2005), was performed in order to check the reliability of the GCM-forced RACMO2 simulations. In this paper, ERA-40 has been used as forcing instead of its successor ERA-Interim (Dee and et al. 2011), since the latter only covered the period 1989–2009 at the time the RACMO2 simulations were started. Other RACMO2 simulations forced by re-analysis data (ERA-40 or ERA-Interim) yielded realistic SMB results over Antarctica

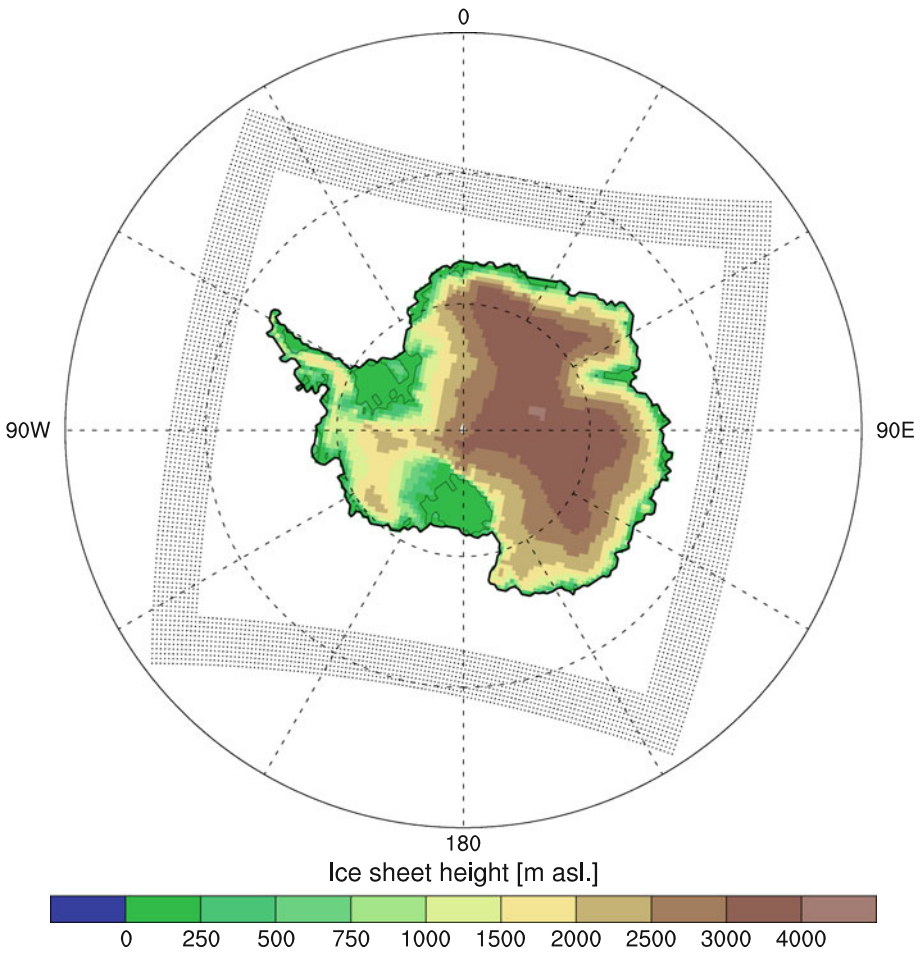

Fig. 1 Map of Antarctica showing the model domain, the boundary relaxation zone (*dotted area*) and model topography in meters above sea level

when compared to in-situ SMB measurements (Van de Berg et al. 2006; Van den Broeke 2008; Lenaerts et al. 2012b). For the purpose of this paper, we therefore consider the RACMO2 SMB field as a benchmark when assessing GCM-forced RACMO2 simulations.

2.3 GCM forcing

Table 1 gives an overview of all simulations performed with RACMO2, their acronym, lateral forcing, emission scenario and time period. In the remainder of this paper, the full name of a GCM (HadCM3 or ECHAM5) is used to refer to direct GCM output, while acronyms starting with "R-" (left column in Table 1) refer to individual RACMO2 simulations.

For the six other simulations (Table 1, except R-ERA), RACMO2 is forced at the lateral boundaries with output from either ECHAM5 or HadCM3; two fully coupled GCMs from the Coupled Model Intercomparison Project [CMIP3, as used in IPCC (2007)]. Data of these models have been made available through the ice2sea project. ECHAM5 contains the latest cycle of the European Centre/Hamburg model version 5 for the atmosphere and the Max Planck Institute Ocean Model (MPI-OM) for the ocean (Muller and Roeckner 2007). For HadCM3, that contains the atmospheric model HadAM3 (Pope et al. 2000) and the ocean model HadOM3 (Gordon et al. 2000), we use the model version that was used in the ENSEMBLES project; HadCM3C (Johns et al. 2011). HadCM3 data are available for 220 years (1980–2199) and ECHAM5 data for 120 years (1980–2099). Both ECHAM5 and HadCM3 have a reasonable horizontal resolution for GCM standards: $3.75° \times 3.75°$ and $2.5° \times 3.75°$ respectively, which translates to $\sim 400 \times 125$ km and $\sim 275 \times 125$ km in Antarctic coastal areas. ECHAM5 and HadCM3 are both preferred forcing models as they perform well in intercomparison and validation studies that focus on the polar regions (Connolley and Bracegirdle 2007; Chapman and Walsh 2007; Franco et al. 2011; Maris et al. 2012).

Table 1 Overview of RACMO2 simulations (acronyms as used in this paper), their lateral forcings, emission scenarios and the time period covered

Simulation acronym	Model forcing	Scenario	Time period
R-ERA	ERA-40	20c	1980–1999
R-H3	HadCM3	20c	1980–1999
R-E5	ECHAM5	20c	1980–1999
R-E5-A1B	ECHAM5	A1B	2000–2099
R-E5-E1	ECHAM5	E1	2000–2099
R-H3-A1B	HadCM3C	A1B	2000–2199
R-H3-E1	HadCM3C	E1	2000–2199

Two different greenhouse gas emission scenarios are considered: A1B and E1. In the IPCC SRES A1B scenario, fossil fuel emissions double in 2050, compared to 1990, and CO_2 concentrations rise to roughly 700 ppmv (Nakicenovic et al. 2000). As a consequence, the GCM ensemble in IPCC AR4 predict average global 2 m air temperature (T_{2m}) to rise by 2.8 K, with a likely range of 1.7–4.4 K, in the twenty first century (IPCC 2007). A1B is a moderate emission scenario and represents the middle to high temperature rise as predicted by IPCC AR4. The A1B scenario is only defined until 2100; for post-2100 simulations CO_2 concentrations are considered to remain constant at their 2100-level ($\sim$900 ppmv). The European ENSEMBLES project E1 scenario is a strong mitigation scenario. It follows the European Union climate policy, stating that a 2 K rise in global T_{2m} compared to pre-industrial levels should be considered a maximum acceptable temperature rise. In the E1 scenario, CO_2 concentrations are therefore restricted to peak at 530 ppmv around 2050 and slowly decrease afterwards (Lowe et al. 2009).

Figure 2 shows global (thick lines, left axis) and Antarctic (thin lines, right axis) average T_{2m} for the next two centuries as simulated by the HadCM3 model. In the E1 scenario, global T_{2m} reaches its maximum increase of 1.7 K in 2070, so it remains below the upper boundary imposed for this emission scenario. After 2070, temperatures remain rather constant, with even a slight negative trend in the late twenty second century. In the A1B scenario, global T_{2m} shows a more pronounced rise of 4.0 K in the twenty first century, and the warming stabilizes around +5.4 K in 2130. The HadCM3 simulated temperature rise exceeds the average IPCC global temperature rise (+2.8 K in 2100). For both scenarios, the AIS averaged T_{2m} follows the same pattern of temperature increase and stabilization afterwards. The simulated temperature rise in ECHAM5 until 2100 is similar to that found in HadCM3 (not shown).

3 Results: current climate

3.1 Temperature

For the period 1980–1999, Table 2 lists the simulated Antarctic climate of the GCM-forced RACMO2 simulations R-H3, R-E5, the RACMO2 benchmark simulations R-ERA and the direct GCM output of HadCM3 and ECHAM5. Annual ice sheet average T_{2m} in both R-H3 (−1.5 K) and R-E5 (−2.0 K) is lower than in R-ERA (Fig. 3; Table 2). The inter-annual variability in the reference period, given as the standard deviation in Table 2, is similar for the three historical RACMO2 simulations (R-ERA, R-H3 and R-E5). The average temperature in the vertical atmospheric column (T_{atm}) is also lower, with

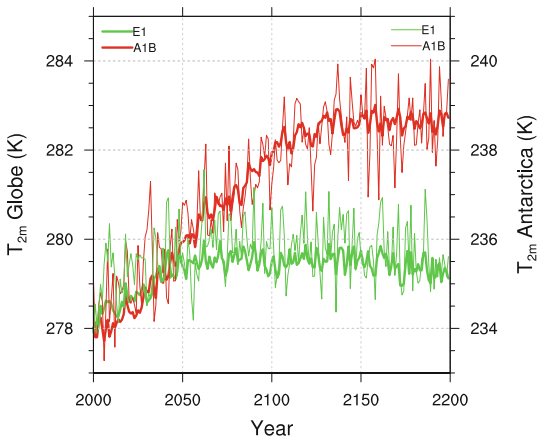

Fig. 2 Time series (2000–2199) of globally averaged (*thick lines*, *left axis*) and Antarctic averaged (*thin lines*, *right axis*) 2 m air temperature (T_{2m}) as simulated by HadCM3 for the A1B (*red*) and E1 (*green*) emission scenarios

R-H3 (−2.6 K) yielding smaller differences than R-E5 (−3.0 K). In both GCM forced simulations (R-H3 and R-E5), T_{2m} shows a spatially uniform negative temperature deviation over the AIS (Fig. 3). R-E5 shows more spatial variation in the difference than R-H3, with differences up to −4 K on the Ross and Filchner-Ronne ice shelves and in West-Antarctica, and the smallest differences in coastal Dronning Maud Land (DML, 75°S, 10°S). A likely cause for the lower T_{2m} in the GCM forced simulations is the lower sea surface temperatures (south of 60°S, −0.2 K in HadCM3 and −0.6 K in ECHAM5), and associated higher sea ice concentrations. This reduces the transport of heat towards the atmosphere over the AIS. The reduced strength of low pressure systems over the Southern Ocean further weakens this meridional heat transport, as will be discussed later in in this section.

3.2 Surface mass balance (SMB)

All SMB components are underestimated by R-E5 and R-H3, compared to R-ERA (Table 2), due to the lower simulated temperatures in the GCM-forced simulations, as colder air has less water vapor holding capacity than warmer air. Snowfall amounts are therefore lower in the GCM-forced simulations (R-H3 −14 % and R-E5 −19 %). The larger temperature deviation in R-E5 is reflected in a larger snowfall difference. Also rainfall, sublimation, and snowmelt are underestimated due to the cold biases in R-E5 and R-H3 (Table 2). The reduction of available liquid water from rainfall and snowmelt leads to lower refreezing and runoff amounts in R-E5 and R-H3. Runoff is a small SMB component in R-ERA ($\sim$10 Gt year^{-1}) and almost absent in R-H3 and R-E5. It should be noted that the average runoff values in all historical RACMO2 simulations (R-E5, R-H3 and R-ERA) are lower due to model spin-up: the snow pack in RACMO2 is initialized without liquid or refrozen meltwater and the model takes $\sim$10 years to adjust (Ettema 2010), especially in areas where liquid water processes are important (e.g. the Antarctic Peninsula). However, as runoff on Antarctica is small, the impact on the SMB is minor. All in all, we find lower SMB values in R-H3 (−14 %) and R-E5 (−19 %) compared to R-ERA. These values again show that differences in snowfall almost fully determine differences in SMB.

Figure 4a shows the spatial distribution of the AIS SMB in R-ERA, which is similar to the spatial pattern found by Van de Berg et al. (2006) and Lenaerts et al. (2012a). It also resembles the range of simulated SMB values (<20 mm year^{-1} in a large part of East Antarctica and up to 2,000 mm year^{-1} on the Antarctic Peninsula). Figure 4b, c show the spatial differences in SMB between

Table 2 RACMO2 output, forced by ERA-40 (R-ERA), ECHAM5 (R-E5) and HadCM3 (R-H3) and direct GCM output (ECHAM5 and HadCM3). Listed are 20-year (1980–1999) ice sheet averages and corresponding standard deviations for T_{2m}, T_{atm}, snowfall, rainfall, total precipitation, sublimation, snowmelt, refreezing, runoff and SMB. Temperatures are given in [K] and the SMB components in [Gt yr-1]

Variable	R-ERA	R-E5	ECHAM5	R-H3	HadCM3
T_{2m}	235.0 ± 0.6	233.0 ± 0.7	233.1 ± 0.5	233.5 ± 0.7	234.3* ± 0.5
T_{atm}	228.5 ± 0.5	225.5 ± 0.4		225.9 ± 0.7	
Snowfall	2421 ± 97	1957 ± 57		2083 ± 89	
Rainfall	27.5 ± 6.7	12.8 ± 4.5		18.2 ± 5.9	
Precipitation	2448 ± 97	1970 ± 58	2428 ± 81	2101 ± 90	2381 ± 118
Sublimation	75.8 ± 7.2	64.3 ± 8.6	7.6 ± 3.5	61.5 ± 7.7	175 ± 8.7
Snowmelt	100.3 ± 23.4	55.5 ± 28.5		46.0 ± 15.6	
Refreezing	123.5 ± 25.1	68.1 ± 32.6		64.0 ± 19.7	
Runoff	4.3 ± 4.3	0.3 ± 0.4	0.0 ± 0.0	0.2 ± 0.3	171 ± 37
SMB	2353 ± 97	1896 ± 57	2421 ± 81	2029 ± 88	1988 ± 132

* HadCM3 output represents 1.5 m temperature

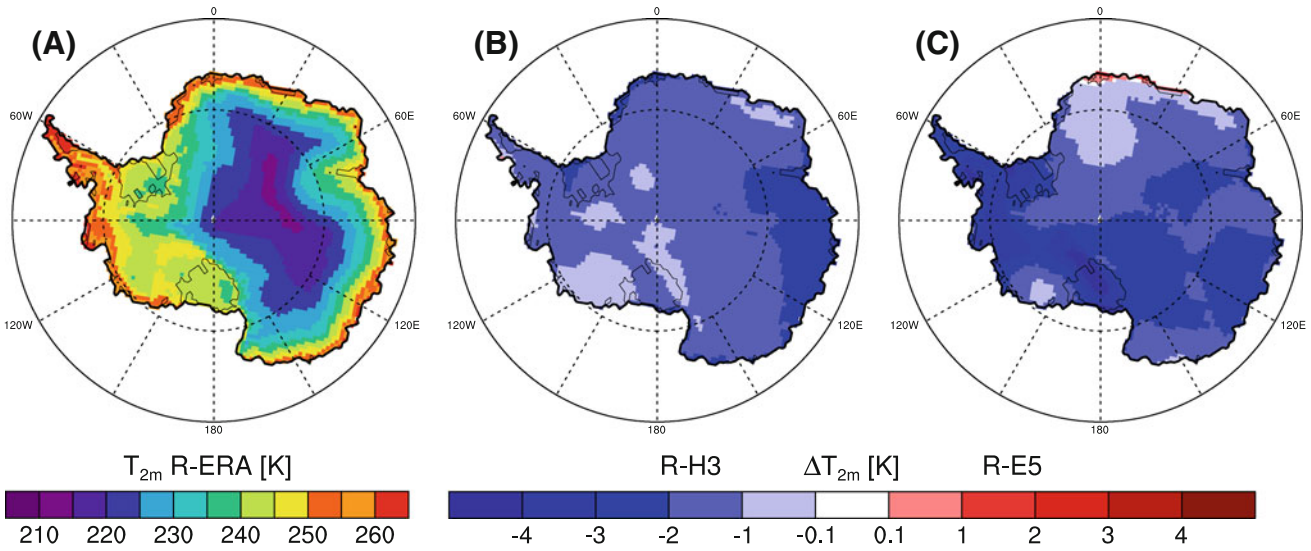

Fig. 3 Spatial distribution (1980–1999 average) of 2 m temperature (T_{2m}) for R-ERA (**a**) and the difference in T_{2m} between R-H3 and R-ERA (**b**) and R-E5 and R-ERA (**c**)

the GCM-forced simulations (R-H3 and R-E5) and R-ERA. The differences are generally within 10 % of the total SMB; large increases are found on the Ross Ice Shelf and its vicinity and in parts of coastal DML, while the largest negative deviations are found in Wilkes Land and West Antarctica. These patterns are caused by differences in the surface pressure (p_{surf}) distribution around Antarctica (Fig. 4d–f). There are typically three climatological low pressure centers located around Antarctica; (i) in the Amundsen Sea, (ii) off the coast of DML and (iii) off the coast of Wilkes Land (Fig. 4d), as described by Van den Broeke and Van Lipzig (2004). These low pressure centers determine the location and strength of the meridional transport of heat and moisture onto the AIS. In both R-H3 and R-E5, the low pressure systems are less pronounced than in R-ERA, regionally resulting in less transport of moisture towards the AIS. For example, lower snow accumulation/SMB in West-Antarctica can be attributed to a weaker Amundsen Sea low pressure system: 980.8 hPa in R-ERA, 981.5 hPa in R-H3 and ~985 hPa in R-E5 (in the latter model, there is no distinct low pressure center in the Amundsen Sea). Simultaneously, the flow off the ice-sheet around the Ross Ice Shelf is also weakened and as a result moist air from the ocean will more often flow onto the ice sheet, leading to more precipitation in this region. For R-E5, p_{surf} differences are larger, compared to R-H3, resulting in larger SMB differences, however the spatial patterns are similar to R-H3.

3.3 RACMO2–GCM comparison

Direct GCM output lacks the resolution and realistic snow physics to accurately capture the individual SMB components (Table 2). In ECHAM5, precipitation and SMB are virtually equal, as no runoff is simulated and sublimation is an order of magnitude smaller than in RACMO2 (8 vs. 76 Gt year^{-1}). The latter is mainly caused by ECHAM5's coarse meridional resolution (~400 km) in the steep coastal area (Fig. 5b), where most sublimation takes place. In HadCM3, precipitation is higher than in R-ERA, however this is compensated by an overestimation of sublimation (165 vs. 76 Gt year^{-1}) and runoff (165 vs. 10 Gt year^{-1}). Especially the latter is unrealistically high, as in reality runoff hardly occurs in Antarctica (Lenaerts et al. 2012a).

In Fig. 5 the impact of the difference in grid resolution between GCM and RACMO2 output is clearly visible. R-E5 and R-H3 show more spatial detail in the SMB patterns, but qualitatively the overall spatial distribution in HadCM3 is quite good; with the highest SMB values occurring along the West-Antarctic coast and the western Antarctic Peninsula, and lower values in DML and Victoria Land (80°S, 150°E). ECHAM5's coarser meridional resolution precludes resolving these spatial details. Both GCMs overestimate the SMB in the AIS interior. Also note that both GCMs have problems near the geographical South Pole. HadCM3 simulates hardly any precipitation in these grid boxes, leading to a negative SMB, while ECHAM5 on the other hand simulates more precipitation on the eastern side than in the surrounding grid boxes, which also leads to an unrealistic spatial SMB pattern.

Figure 6 shows that the GCMs simulate a realistic spatial pattern for near-surface temperature and the AIS average value is in the same range as the three RACMO2 simulations (R-ERA, R-E5 and R-H3). Both GCMs simulate the correct T_{2m}-range between the East-Antarctic plateau and coastal areas (215–250 K). In areas with more

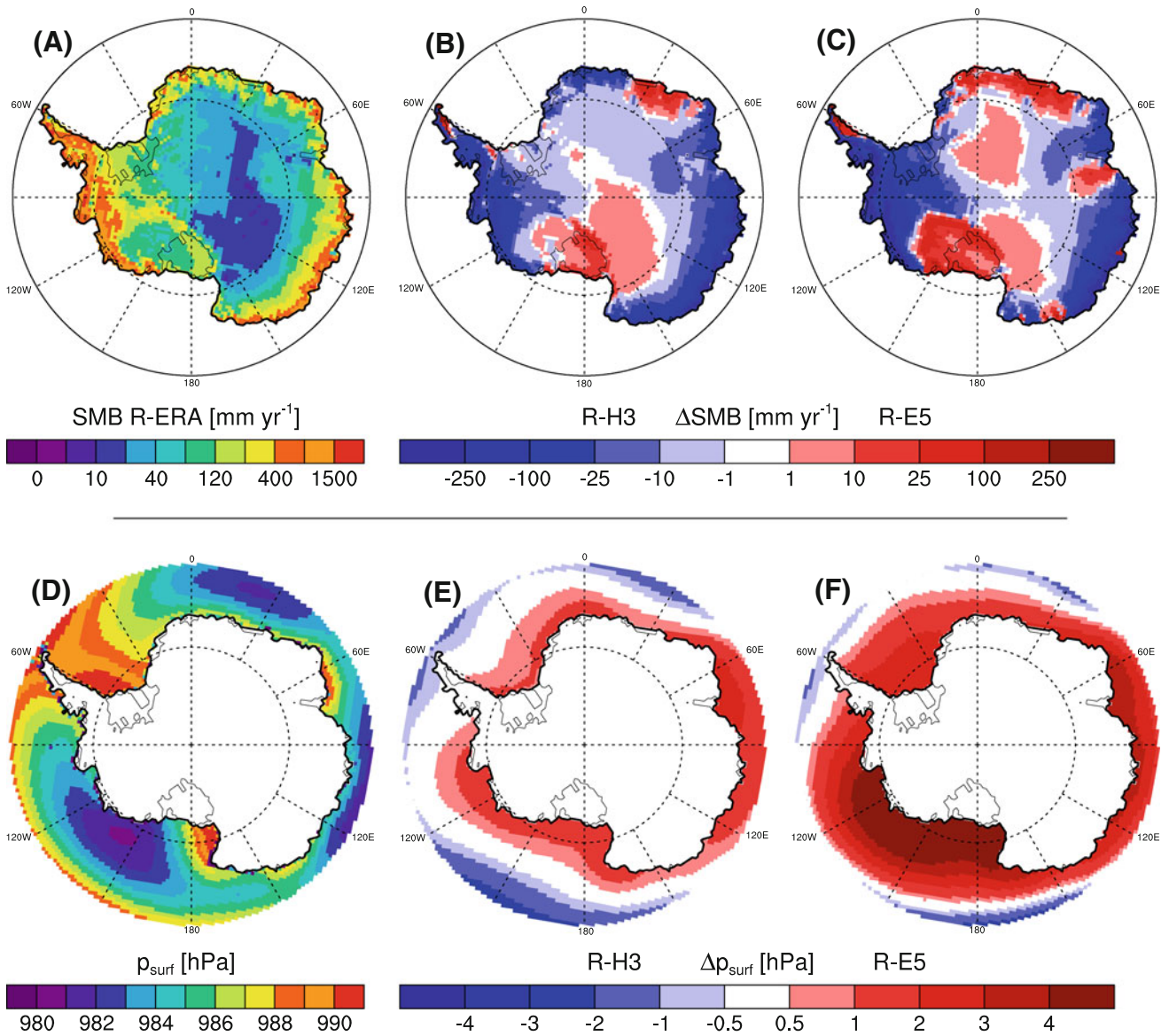

Fig. 4 Spatial distribution (1980–1999 average) of SMB (**a**) and surface pressure (p_{surf}) (**d**) for R-ERA and the difference between R-H3 and R-ERA (**b**, **e**) and R-E5 and R-ERA (**c**, **f**) for SMB and p_{surf}, respectively

topographic detail, GCMs overestimate temperature; for example, ECHAM5 overestimates T_{2m} in the northern Antarctic Peninsula and both GCMs overestimate T_{2m} over the large ice shelves (Ross and Filchner-Ronne), an indication that topography is smoothed and on average lower.

In summary, both GCM-driven RACMO2 simulations (R-H3 and R-E5) are colder and drier than R-ERA. Reasons for these deficiencies are underestimated SST, overestimated sea ice cover and less pronounced low pressure systems along the Antarctic coast, the latter being the main source of meridional heat and moisture transport onto the ice sheet. In both R-H3 and R-E5, relative inter-annual variability of the SMB components is in the same range as R-ERA (Table 2). For snowfall, the most important SMB component, the R-H3 simulation is closer to R-ERA than the R-E5 simulation, as well in absolute amounts as in inter-annual variability. Moreover, HadCM3 provides forcing data until 2200 compared to 2100 for ECHAM5; in the next section, we will therefore mainly discuss the results of RACMO2 simulations forced with HadCM3. The absolute differences (Table 2) between the three RACMO2 simulations are smaller than the RACMO2-GCM and inter-GCM differences (Maris et al. 2012). Although both GCMs predict quite similar AIS average SMB values compared to RACMO2 historical simulations (R-ERA, R-H3 and R-E5), there are compensating errors: both ECHAM5 and HadCM3 simulate sublimation and runoff amounts that are one to two orders of magnitude different from R-ERA.

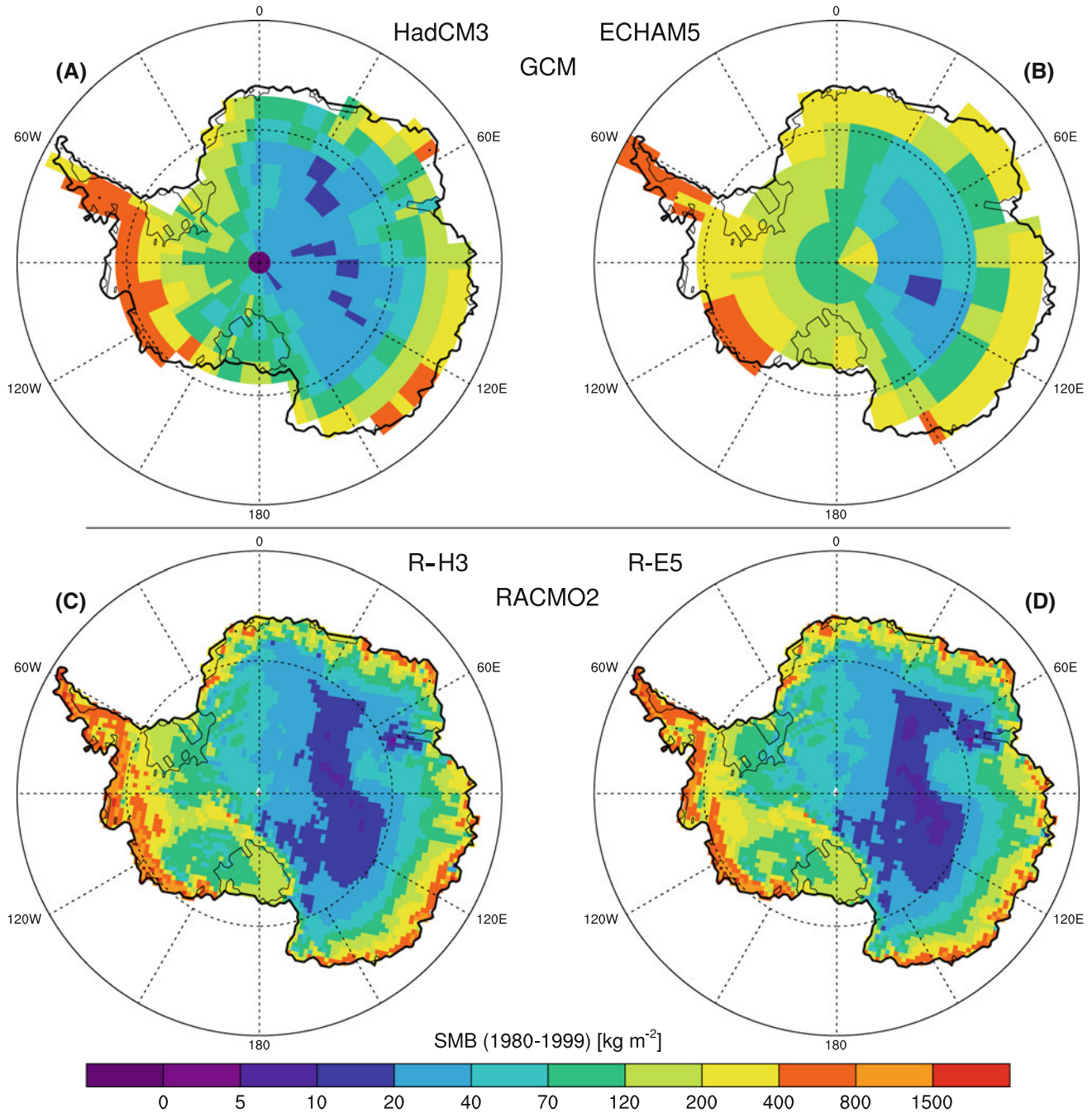

Fig. 5 Spatial distribution (1980–1999 average) of SMB for GCM simulations HadCM3 (**a**) and ECHAM5 (**b**) and RACMO2 simulations R-H3 (**c**) and R-E5 (**d**). RACMO2 grounding line and land contours are used in all figures

4 Results: future climate

4.1 Evolution of T_{2m}

Table 3 shows T_{2m} and SMB-component anomalies for 2080–2099 and 2180–2199 averages of the future RACMO2 simulations (R-H3-A1B, R-H3-E1, R-E5-A1B and R-E5-E1), relative to the 1980–1999 average of R-H3 or R-E5. Temperature increases of 3.0 K (R-H3-A1B) and 2.0 K (R-H3-E1) in 2100 and 5.3 K and 2.4 K in 2200 are simulated (Fig. 7a), similar to the GCM simulated warming (Fig. 8a). However, Fig. 7a shows that R-H3-A1B reaches the stabilization temperature later in the twenty second century than HadCM3 in Fig. 2. Still, the final value of the temperature rise is similar: +5.3 and +5.4 K in 2200. Also the variability in T_{2m} is similar in HadCM3 and R-H3-A1B (Figs. 2, 7a). A possible explanation for the warming lag between a GCM and RACMO2 could be

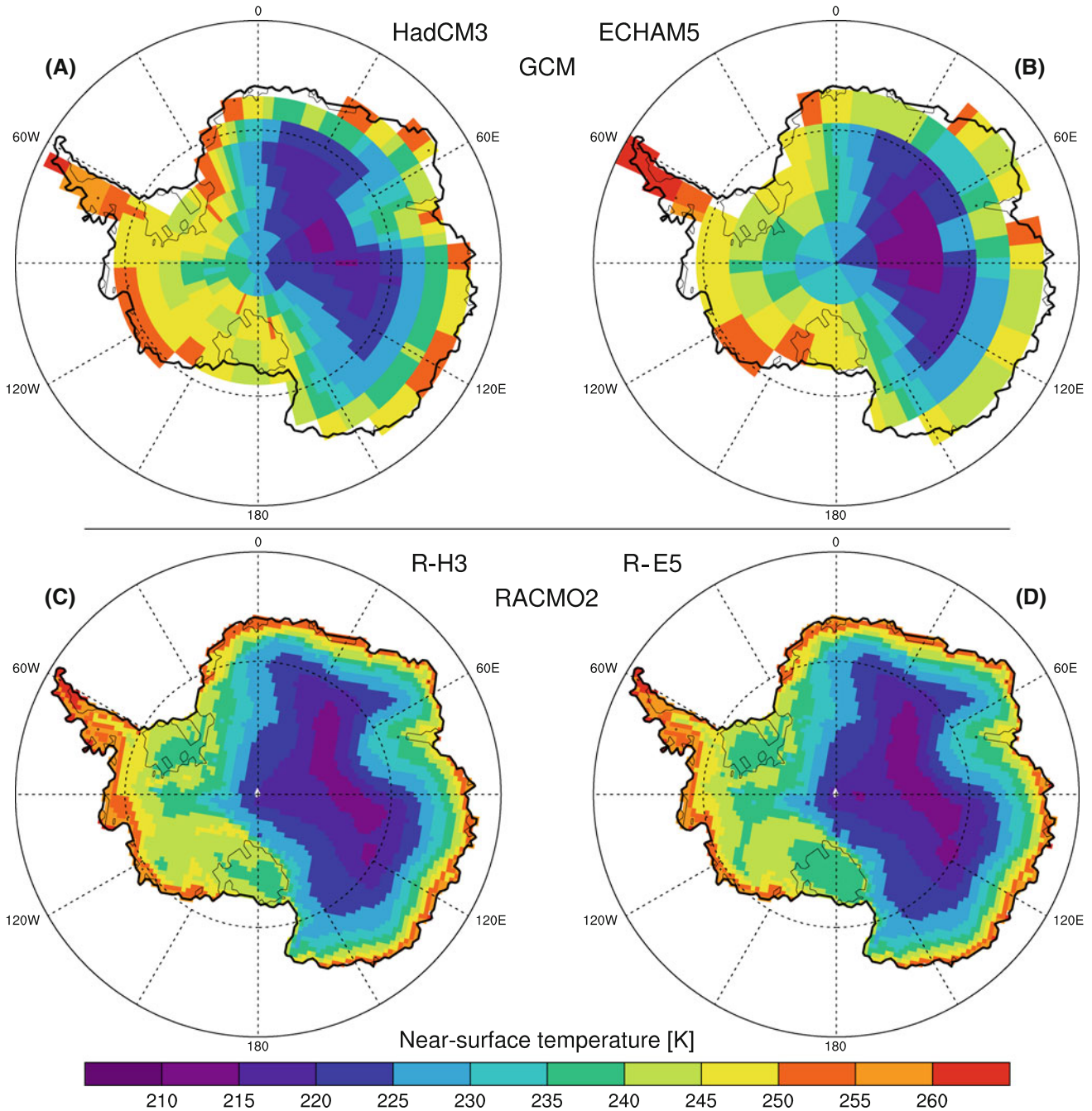

Fig. 6 Spatial distribution (1980–1999 average) of near-surface temperature for GCM simulations HadCM3 (**a**) and ECHAM5 (**b**) and RACMO2 simulations R-H3 (**c**) and R-E5 (**d**). RACMO2 grounding line and land contours in all figures. Near-surface temperature is 2 m temperature (T_{2m}) in ECHAM5, R-H3 and R-E5, and 1.5 m temperature in HadCM3

found in differences in model physics and parameterizations. For example, the use of more vertical layers to resolve the snowpack and the application of a more realistic albedo parameterization in RACMO2 makes the albedo more sensitive to snowfall events. With future increasing snowfall, this mechanism could slow down the temperature increase near the surface (Picard et al. 2012). Also, the difference in horizontal grid size between GCM and RACMO2 could act as a temperature buffer along the coastal margins of the AIS. Rising temperatures in these regions can affect a greater area in GCMs, due to the larger grid cells, and thereby trigger temperature-snowmelt-albedo feedbacks. These feedbacks are also present in RACMO2, only on much smaller scales.

For the E1 scenario, HadCM3 (Fig. 2) follows the T_{2m} increase of the A1B simulation until 2050, as is the case in

R-H3-E1 (Figs. 7a, 8a). After this, HadCM3 T_{2m} remains rather constant for the remainder of the simulation period, and the warming remains below the +2 K threshold (Fig. 2). In R-H3-E1 however, there is a second warming episode at the end of the twenty second century, increasing T_{2m} above the +2 K threshold. This is likely caused by the same time lag effect as in the A1B simulations, however less pronounced due to a smaller amplitude in temperature change. For both future R-E5 simulations, the T_{2m} increase in 2100 is similar [+1.8 K (E1) and +2.9 K (A1B)] to the future R-H3 simulations. In none of the future simulations is relative inter-annual variability found to change significantly with time.

Figure 9b, c show that the temperature rise in the twenty first century is uniform across the entire AIS for both emission scenarios. In both cases the temperature increase varies by 0.5 K from the average increase; 2.5–3.5 K (A1B) and 1.5–2.5 K (E1). In general, the temperature increase along the coastal margins is slightly larger than in the interior. On the East-Antarctic plateau (80 °S, 90 °E) a numerical artifact is visible. At this location, which receives very low accumulation, the snow in the upper RACMO2 model layer is refreshed too slowly, causing unrealistically large snow grain sizes and therefore a too low albedo. However, the effect on AIS average T_{2m} is minor ($\sim$0.02 K).

Table 3 Difference in absolute (Gt year^{-1}) and relative (%) amounts between RACMO2 future simulations (R-E5-A1B, R-E5-E1, R-H3-A1B, R-H3-E1) and 1980–1999 simulations (R-E5 and R-H3, respectively). Listed are differences between 2080–2099 and 1980–1999 20-year ice sheet averages for T_{2m}, snowfall, SMB, sublimation, rainfall, snowmelt, runoff and refreezing. Temperatures are given in [K] and the SMB components in [Gt yr-1]. The second row in the H3 results show the differences between 2180–2199 and 1980–1999 averages. For runoff no relative differences are shown as the 1980–1999 averages are close to zero

Variable	R-E5-A1B	R-E5-E1	R-H3-A1B	R-H3-E1
T_{2m}	+2.9	+1.8	+3.0	+2.0
			+5.3	+2.4
Snowfall	+287 (15 %)	+105 (5.4 %)	+353 (17 %)	+144 (6.9 %)
			+551 (26 %)	+176 (8.4 %)
SMB	+265 (14 %)	+ 84 (4.4 %)	+334 (16 %)	+124 (6.1 %)
			+508 (25 %)	+157 (7.7 %)
Sublimation	+24.6 (38 %)	+19.6 (30 %)	+24.6 (40 %)	+19.7 (32 %)
			+54.0 (88 %)	+25.9 (42 %)
Rainfall	+12.7 (99 %)	+4.8 (38 %)	+28.9 (159 %)	+11.6 (64 %)
			+54.8 (301 %)	+16.0 (88 %)
Snowmelt	+70.6 (127 %)	+33.3 (60 %)	+84.1 (183 %)	+61.8 (134 %)
			+164 (356 %)	+47.8 (104 %)
Runoff	+8.7	+6.3	+21.5	+11.4
			+39.4	+8.9
Refreezing	+74.5 (109 %)	+32.0 (47 %)	+92.0 (144 %)	+62.0 (97 %)
			+179 (280 %)	+54.9 (86 %)

4.2 Evolution of the SMB

Figure 7b–h show the evolution of the SMB components for the four GCM forced RACMO2 simulations. In general, the hydrological cycle of the AIS intensifies in a warmer Antarctic climate. Snowfall increases by 26 % in R-H3-A1B, from $\sim$2,100 Gt year^{-1} in R-H3 to $\sim$2,650 Gt year^{-1} in 2200, while R-H3-E1 shows a more moderate increase of 8 % by 2200 (Fig. 7b; Table 3). In both scenarios, snowfall and T_{2m} appear linked: periods with increasing and stabilizing T_{2m} coincide with periods of increasing and stabilizing snowfall (Fig. 7a, b). Figure 8a, b emphasize the casual relation between rising temperatures and increasing precipitation in both GCM and RACMO2 simulations. A strong increase in T_{2m} (e.g. around 2050 in the A1B simulations) is accompanied by a rapid precipitation increase. Also, a reduction in T_{2m} increase (e.g. around 2070 in the A1B simulations) translates into a reduced precipitation increase. For the E1-simulations, the relation between rising temperatures and increasing precipitation is also evident, however, due to the smaller increase in T_{2m} the signal is more variable.

The spatial pattern of snowfall (or SMB) increase over the twenty first century shows the same relation between temperature and precipitation (Fig. 10b, c). The increase is rather uniform over the continent, with the largest increases in West-Antarctica and along the coastal margins, which are both locations with high annual snowfall totals. The uniformity of the increase in both temperature and snowfall suggests that future snowfall changes are mainly caused by increased atmospheric water vapor holding capacity and less by atmospheric circulation changes. For R-H3-E1, a smaller increase in SMB is found (Table 3), which is probably due to the smaller temperature increase (+2.0 K) than in R-H3-A1B (+3.0 K). The future increase in SMB, especially in the strong mitigation scenario simulations (R-E5-E1 and R-H3-E1), is smaller than or similar to the difference in the historical simulations (R-E5/R-H3 vs. R-ERA). This could simply imply that the simulated increase falls within the uncertainty margin. However, it is more likely that the cold and dry bias from the historical

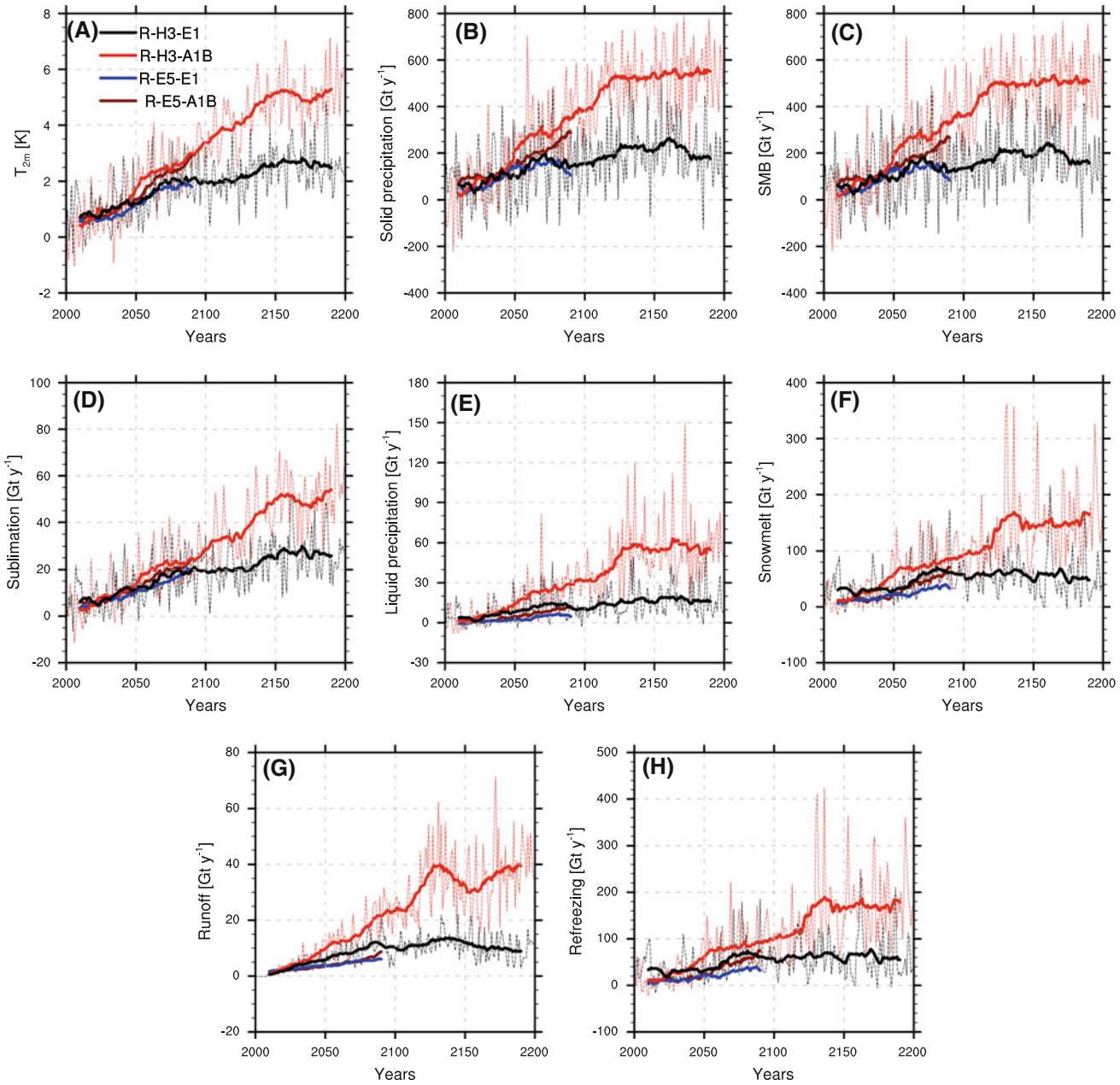

Fig. 7 Time series (2000–2199) of annual and ice sheet averaged T_{2m} (**a**), solid precipitation (**b**), SMB (**c**), sublimation (**d**), liquid precipitation (**e**), snowmelt (**f**), runoff (**g**) and refreezing (**h**), for four RACMO2 simulations; R-E5-A1B (*brown*), R-E5-E1 (*blue*), R-H3-A1B (*red*) and R-H3-E1 (*black*), relative to the 1980–1999 average values of R-E5 and R-H3 respectively. For all four simulation 20-year running averages (*solid*) and for both H3 simulations also annual averages (*dashed*) are shown

runs is also present in the future simulations. As will be shown in Sect. 4.3, there is a strong linear relation between temperature and snowfall/SMB in Antarctica, indicating that SMB will rise with temperature independent of the starting conditions (as long as these fall within a realistic range).

In Figure 10e, f, the relative differences in p_{surf} over the twenty first century show no large deviations from the average R-H3 pattern, as was the case for SMB (Fig. 10b, c). In both simulations, the differences in p_{surf} between R-H3-A1B/R-H3-E1 and R-H3 (Fig. 10e, f) are smaller than between R-ERA and R-H3 (Fig. 4e). This confirms that the differences in SMB (Fig. 10b, c) are mainly influenced by temperature changes and less by circulation changes.

In the present climate, rainfall only occurs along the coastal margins of the AIS, roughly below 1,000 m asl., and on the ice shelves. In R-H3-A1B, rainfall increases by

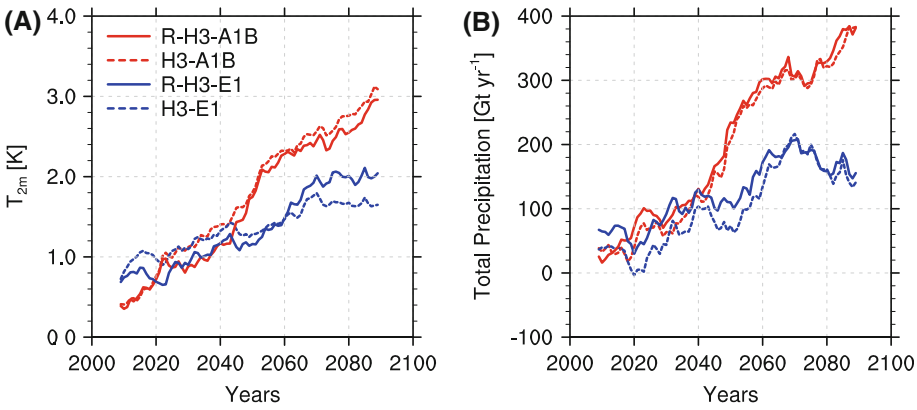

Fig. 8 Time series (2000–2099) of 20-year, ice sheet averaged T_{2m} (**a**) and total precipitation (**b**) for RACMO2 simulations; R-H3-A1B (*red*, *solid*) and R-H3-E1 (*blue*, *solid*) and GCM simulations; H3-A1B (*red*, *dashed*) and H3-E1 (*blue*, *dashed*), relative to the 1980–1999 average values of R-H3 and HadCM3 respectively

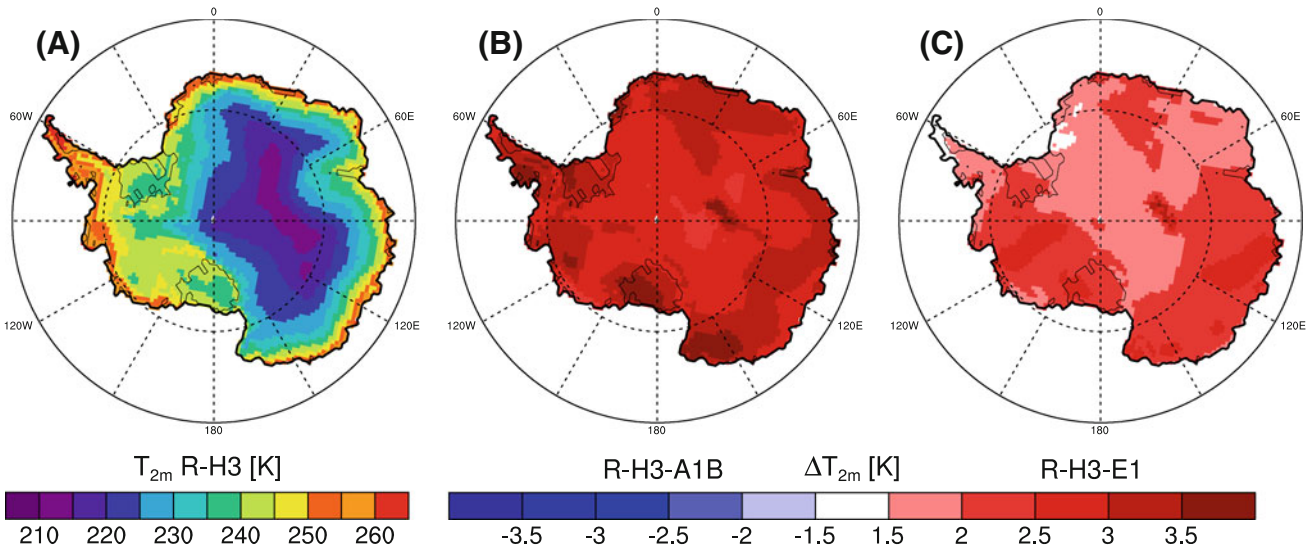

Fig. 9 Spatial distribution of R-H3 1980–1999 T_{2m}-average (**a**), the difference between R-H3-A1B 2080-2099 T_{2m}-average and **a** (**b**) and R-H3-E1 2080–2099 T_{2m}-average and **a** (**c**), respectively

more than 50 Gt year^{-1} in the next two centuries, a threefold increase from R-H3 simulated rainfall (Fig. 7e; Table 3). Our results show only minor changes in the spatial rainfall distribution, most likely because the ice sheet is rather steep in the coastal regions, preventing the penetration of warmer near surface temperatures inland. In R-H3-E1, the increase is less pronounced and stabilizes around 16 Gt year^{-1} ($\sim$80 %). The relative inter-annual variability in rainfall, taken as the ratio of the standard deviation and the mean absolute value, is strongly influenced by a few peak years, but shows no significant trend.

In R-H3-E1, snowmelt evolution shows the same increase and stabilization as rainfall; amounts roughly double during the twenty first century and remain constant afterwards. In the A1B simulation, snowmelt increases more strongly, with an increase of 80–85 Gt year^{-1} in both the twenty first and twenty second century (Fig. 7f; Table 3). As with rainfall, inter-annual variability is strongly influenced by a few peak years, but there is no significant trend. The peak years around 2130, in which annual snowmelt exceeds 400 Gt year^{-1}, are remarkable.

The increase in liquid water flux from enhanced rainfall and snowmelt is not reflected in high runoff rates (Fig. 7g), as most liquid water refreezes in the snow pack (Fig. 7h). In R-H3-A1B, the liquid water flux increases with more than 200 Gt year^{-1} in 2180–2199 (Table 3). Runoff only increases by 40 Gt year^{-1}, so most of the additional rainfall is a positive contribution to the SMB of the AIS. In R-H3-E1, runoff follows the same temporal pattern as snowmelt, i.e. an increase until 2100 and stabilization afterwards. Values remain low. In both emission scenarios, future runoff occurs only on ice shelves in the Antarctic Peninsula (Larsen C, Wilkins and George VI), which is also reflected in decreasing SMB values in these regions (Fig. 10b). As snowmelt is underestimated by $\sim$50 % in R-E5 and R-H3, compared to R-ERA (see Table 2), snowmelt and related runoff estimates in the future RACMO2 simulations are also likely to be underestimated. For runoff, this will

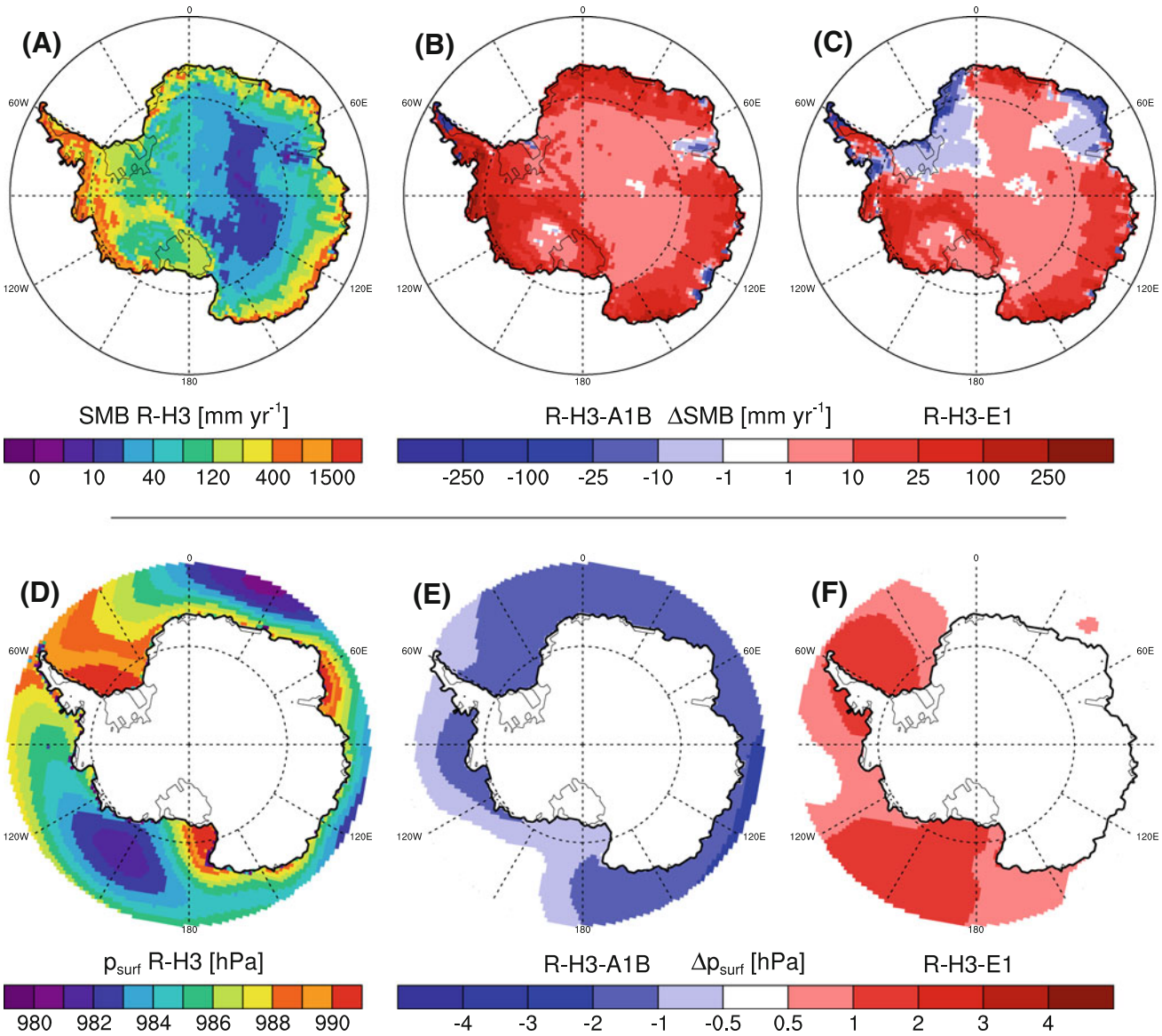

Fig. 10 Spatial distribution of SMB (**a**) and surface pressure (p_{surf}) (**d**) for R-H3 (1980–1999 average), the difference between R-H3-A1B 2080-2099 SMB-average and **a** (**b**), R-H3-E1 2080–2099 SMB-average and **a** (**c**), R-H3-E1 2080–2099 p_{surf}-average and **d** (**e**) and R-H3-E1 2080–2099 p_{surf}-average and **d** (**f**), respectively

probably have a minor effect, because of the large available refreezing capacity on the AIS and the linear relation between T_{2m} and SMB, as will be discussed later.

As T_{2m} increases, sublimation of surface snow also increases due to the greater snow-to-atmosphere moisture gradient (Fig. 7d). Higher temperatures in the A1B scenarios lead to larger sublimations increases (+88 %) than in the E1 scenario (+42 %). During 2000–2099, the increase in sublimation is rather uniform in all four RACMO2 simulations. Thereafter, sublimation increases in R-H3-A1B at the same rate until 2150, while in R-H3-E1 sublimation only shows a minor increase during the twenty second century. Surface sublimation is a relatively constant process, and relative inter-annual variability remains constant during the full simulation period: ~10 % of the total sublimation.

In summary, the T_{2m} increase strengthens the AIS hydrological cycle, however the increase in surface mass loss components is by far outweighed by the increase in mass influx from precipitation. Sublimation increases by 25–50 Gt year^{-1} in the next 200 years, and while rainfall and snowmelt occasionally exceed 200 and 400 Gt year^{-1}, almost all of this liquid water refreezes in the snowpack. As a result, runoff values remain low and hardly influence the SMB. Therefore, the temporal and spatial patterns of SMB changes are very similar to that of snowfall: +26 %

in A1B and +8 % in E1 in 2180–2199 (Fig. 7c) compared to the 1980–1999 averages in R-H3. No significant trend in relative inter-annual variability is found. The R-E5-A1B and R-E5-E1 simulations (not shown) show results and trends similar to the respective H3 future simulations.

4.3 Influence on future sea level

Figure 11 shows sea level change resulting from the cumulative SMB anomaly (Fig. 7c) relative to the 1980–1999 average SMB of the corresponding simulation. To estimate sea level change from SMB, only grounded ice-sheet totals are used. For the R-H3-A1B scenario, a total cumulative SMB anomaly of $+59 \cdot 10^3$ Gt in 200 years is found, corresponding to a sea level drop of 163 mm in 2200 (using 360 Gt water equivalent to equal 1 mm eustatic sea level change). For the twenty first century, a sea level drop of 43 mm is found. In the R-E5-A1B scenario, a potential sea level drop of 32 mm is simulated for the twenty first century, slightly lower than the value found in R-H3-A1B. This difference represents part of the uncertainty that is introduced by the choice of forcing models. For E1, the strong mitigation scenario, a potential sea level drop of 20 mm (R-E5-E1) and 27 mm (R-H3-E1) is found for the twenty first century (Fig. 11). Uncertainties in the simulated Antarctic SMB are estimated at $\sim$10 % (Rignot et al. 2008), so error bars in Fig. 11 are calculated by using 90 and 110 % of the SMB anomalies.

Models without explicit SMB calculation, such as ice-dynamical models or simplified global climate models, often make use of a relation between the change in T_{2m} (ΔT_{2m}) and the change in SMB (ΔSMB). For R-H3-A1B, this SMB sensitivity (given in Gt w.e. year^{-1} K^{-1}, as in Van Lipzig et al. (2002) among others) is shown in Fig. 12, and is based on the strong linear relations between annual ice sheet averaged T_{2m}, SMB and the total precipitable water (PW) in the atmosphere above the ice sheet (in Gt w.e.). The strong linear relation between T_{2m} and PW with a positive slope of 1.25 Gt w.e. K^{-1} indicates an 6–8 % increase of water vapor in the atmosphere per degree warming (Fig. 12a). This is in line with the Clausius-Clapeyron relation (black line in Fig. 12a) that gives an increase of 7 % K^{-1} (Held and Soden 2006). As snowfall is the dominant component of the SMB, a strong PW-SMB relation is expected (Fig. 12b) and combining these two relations, a T_{2m}-SMB relation is derived (Fig. 12c). Owing to the variability of other SMB components (sublimation and runoff), the correlation ($r^2 = 0.69$) in Fig. 12c is lower than found for the relations shown in Fig. 12a, b. The ΔT_{2m}-ΔSMB relation has a positive linear slope of $+97.6 \pm 4.7$ Gt w.e. year^{-1} K^{-1} (or -0.27 ± 0.01 mm SLR year^{-1} K^{-1}). This again confirms that the future increase in Antarctic SMB is mainly driven by an increase

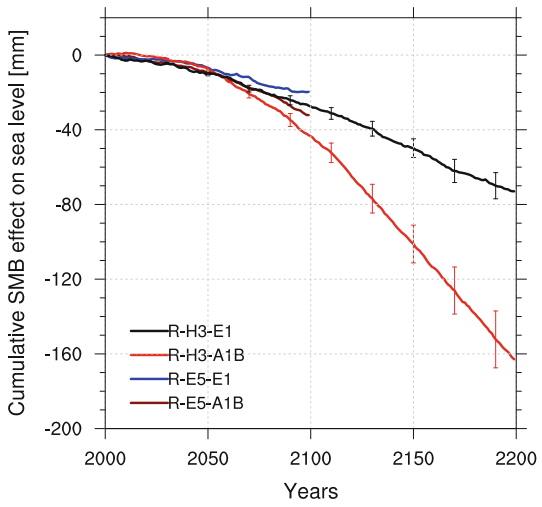

Fig. 11 Cumulative sea level change from grounded AIS SMB anomalies in four RACMO2 simulations; R-E5-A1B (*brown*), R-E5-E1 (EC-E1, *blue*), R-H3-A1B (*red*) and R-H3-E1 (*black*). *Error bars* (only shown for both H3 simulations) indicate the cumulative uncertainty based on Rignot et al. (2008)

in near-surface temperatures and to a lesser degree by changes in atmospheric circulation patterns.

In Table 4, SMB sensitivity and sea level change for the AIS in the twenty first century from this study are compared to results from previous work. All results show a clear increase of SMB with increasing temperature; values vary from 4–9 % K^{-1}. Van Lipzig et al. (2002) reduced the sea ice fraction in their experiment, thereby causing atmospheric circulation to change and generating higher SMB sensitivities. From Fig. 12c we find that the SMB increases with 97.6 Gt K^{-1}, which corresponds to a SMB sensitivity of 4.8 % K^{-1} relative to the 1980–1999 average. The results presented in this study are among the lower estimates of sea level change induced by SMB changes compared to previous studies (Table 4). It should be noted that only sea level change due to SMB changes is considered and it is likely that a part of this change will be counteracted by ice-dynamical effects (IPCC 2007; Rignot et al. 2011; Levermann et al. 2012).

Figure 13a shows that the SMB sensitivity remains partially valid when applied on grid cell scale; roughly half the AIS shows an SMB increase of 15–35 %, which is similar to the AIS averaged SMB sensitivity (Fig. 13b). Using the SMB sensitivity of 4.8 % K^{-1}, the increase in SMB is uniform over the AIS, because it is linearly related to the uniform increase in T_{2m} (Fig. 9). The average increase in SMB is $\sim$25 %, which agrees with the $\sim$5 K temperature rise in R-H3-A1B (Table 3). When the SMB difference between R-H3 and R-H3-A1B is calculated directly (Fig. 13a), more variability is introduced, owing to the temporal and spatial variability in the three SMB components. Apart from a decrease in SMB on the

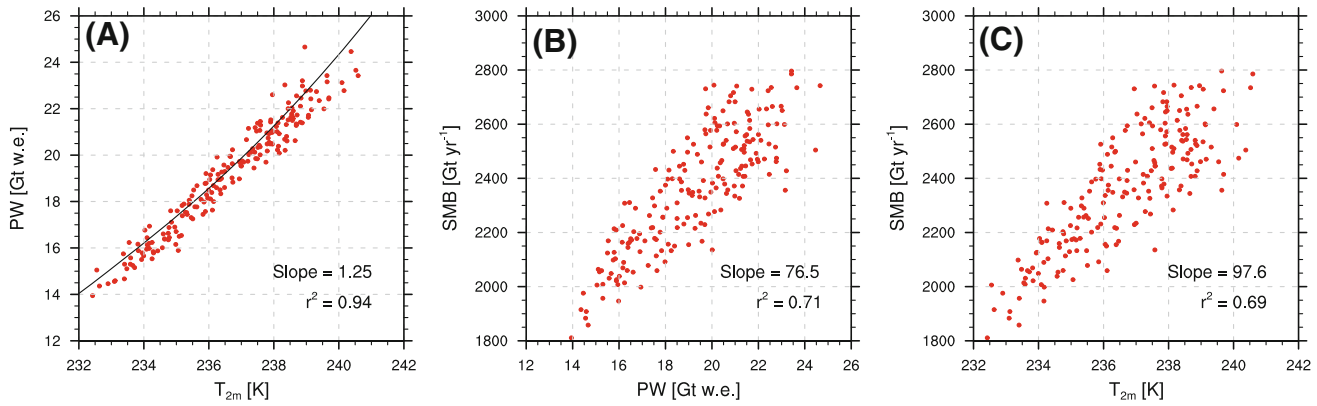

Fig. 12 Relation between total precipitable water (PW) and T_{2m} (**a**), SMB and PW (**b**) and SMB and T_{2m} (**c**), including their slopes and correlation (r^2) for R-H3-A1B. All are annual ice sheet averages and a schematic Clausius-Clapeyron relation (*black*) is shown in **a**, that was obtained with 7 % K^{-1} (Held and Soden 2006), crossing 16 Gt w.e. at 233.8 K

Table 4 SMB sensitivity and sea level drop during the twenty first century for selected studies

References	SMB sensitivity	Sea level drop in twenty first century (mm)
IPCC (2007) AR4	6-9 % K^{-1}	20–120
Van Lipzig et al. (2002)[a]	8.9 % K^{-1}	70
Wild et al. (2003)[b]	7.3 % K^{-1}	45
Gregory and Huybrechts (2006)[c]	~5 % K^{-1}	50
Krinner et al. (2007)[b]	7.1 % K^{-1}	60
Bengtsson et al. (2011)[b]	3.7 % K^{-1}	40
This study	4.8 % K^{-1}	32–43 ± 4

These results were obtained using: [a] present day data from a regional atmospheric climate model simulation (Van Lipzig et al. 2002), [b] high resolution GCM simulations (Wild et al. 2003; Krinner et al. 2007; Bengtsson et al. 2011) or [c] statistical SMB perturbations in GCMs (Gregory and Huybrechts 2006)

Antarctic Peninsula ice shelves, due to increased runoff, precipitation/SMB increases on the rest of the AIS. Along the coastal margins, sublimation increases more rapidly than in the interior of the AIS, leading to larger (>50 %) SMB increases in the interior and smaller (10–20 %) SMB increases along the coastal margins (Fig. 13a). The minor increases near the Filchner-Ronne and Ross ice shelf are caused by a locally lower than average snowfall increase, likely due to atmospheric circulation changes. These results again show that the increase in SMB is in first order determined by temperature increase, and to a lesser extent by atmospheric circulation changes.

5 Discussion and conclusions

The RACMO2 simulations, forced with output from two different GCMs with two different emission scenarios, provide new insights into the future climate and SMB of the AIS. Both GCMs (HadCM3 and ECHAM5) simulate a global T_{2m} rise of ~4 K, larger than the average of the IPCC models (+2.8 K), using emission scenario A1B. In the stronger mitigation emission scenario (E1), both GCMs predict a temperature rise close to 2 K, which is the target of this emission scenario. The simulation of the SMB with RACMO2 provides more detail compared to GCM output. In neither GCM, simulation of the SMB was very realistic; ECHAM5 underestimates sublimation and runoff, while HadCM3 overestimates both these components. However, due to these compensating errors, total SMB values from RACMO2 and GCM output are in the same range.

For the 1980–1999 period, RACMO2 forced with HadCM3 and ECHAM5 output results in a colder and drier Antarctic climate compared to RACMO2 forced with ERA-40 re-analysis. This difference is explained by the lower sea surface temperature and higher sea ice concentrations prescribed from the GCM output, reducing transport of heat and moisture onto the ice sheet.

In most RACMO2 future simulations, the increase in T_{2m} lags that of the GCMs by ~20 years, but reaches the same final value as simulated by the GCMs in 2200. In both emission scenarios, the greenhouse gas emissions and

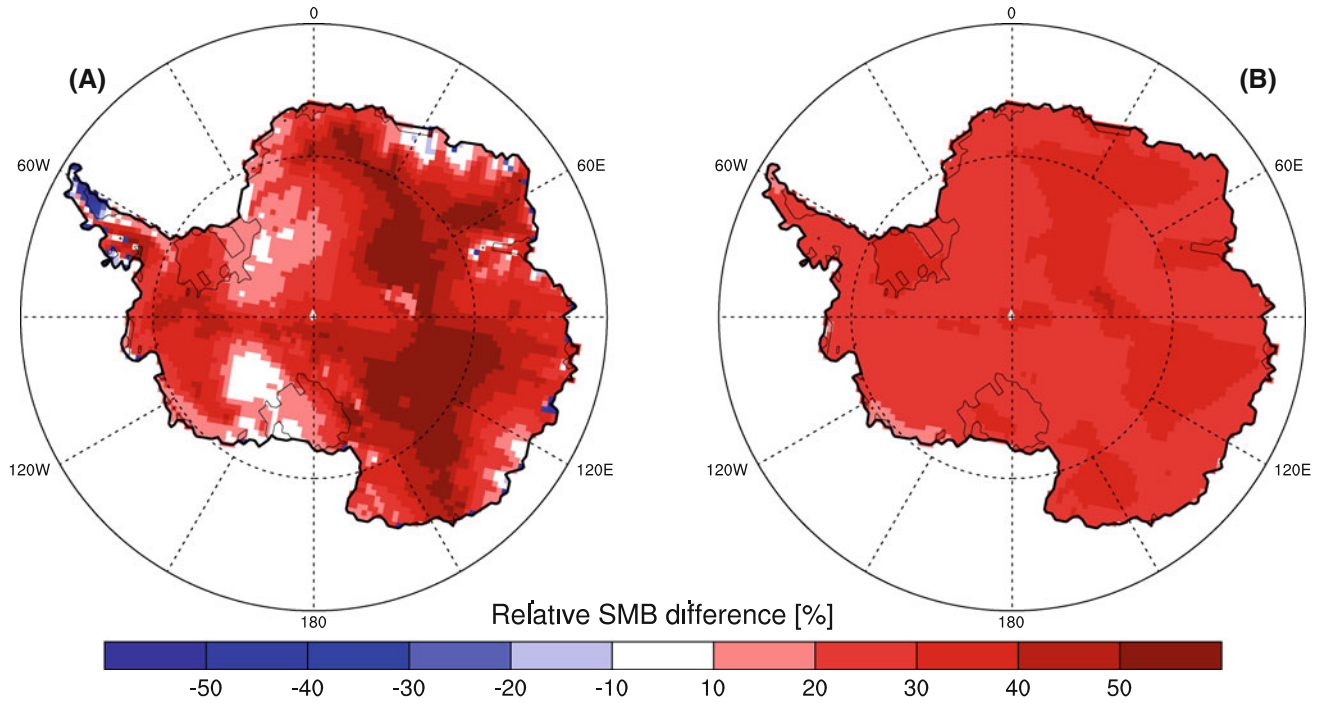

Fig. 13 Relative SMB differences between R-H3-A1B 2180–2199 average SMB and R-H3 1980–1999 average SMB (**a**) and between 2180–2199 average SMB derived using the ΔT_{2m}-ΔSMB relation (Sect. 4.3) and R-H3 1980–1999 average (**b**). For the **b**, ΔT_{2m} was taken as the difference between R-H3-A1B 2180–2199 average T_{2m} and R-H3 1980-1999 T_{2m}

associated atmospheric warming level off in the late twenty second century. The hydrological cycle of the AIS responds strongly to the simulated temperature increase. By 2200, snowfall increases by 550 Gt year^{-1} (26 %) in R-H3-A1B and by 176 Gt year^{-1} (8 %) in R-H3-E1 compared to the R-H3 average. By comparing spatial patterns of twenty first century changes in T_{2m}, SMB and p_{surf}, it is clear that the future SMB changes are mainly caused by the increase in temperature and to a lesser extent by atmospheric circulation changes. Sublimation increases by 25–50 Gt year^{-1}, thereby compensating $\sim$15 % of the increase in snowfall. By 2200, rainfall and snowmelt have strongly increased in low-lying regions of the AIS, by 301 and 356 % (R-H3-A1B) and 88 and 104 % (R-H3-E1), respectively. Most of this additional liquid water refreezes in the snowpack and does not run off; runoff increases to only $\sim$40 Gt year^{-1} in R-H3-A1B and to $\sim$10 Gt year^{-1} in R-H3-E1. So even in a significantly warmer climate, rainfall remains a positive contribution to the SMB of the AIS.

The future SMB change of the AIS is dominated by the increase in snowfall and contributes negatively to global SLR. A significant relation is found between ice sheet averaged ΔT_{2m} and ΔSMB: +97.6 Gt w.e. year^{-1} K^{-1} or -0.27 mm SLR year^{-1} K^{-1}. Changes in mass loss due to ice-dynamical effects will most probably counteract this surface mass gain. When these ice dynamical effects are neglected, our results represent a sea level fall of 32–43 $\pm$ 4 mm (R-H3-A1B) and 20–27 mm $\pm$ 3 (R-H3-E1) in 2100, compared to 1980–1999. For the twenty second century, an additional sea level drop of 46 mm (R-H3-E1) or 120 mm (R-H3-A1B) is predicted.

It is likely that the cold and dry biases in the 1980–1999 simulations persist in the future GCM-forced RACMO2 simulations, as the future simulations are continuations of the historical simulations. However, the impact of this bias can be interpreted relatively easily because of the strong first-order relations in the Antarctic climate: T_{2m}, snowfall and SMB are all closely coupled. Combining that, (i) the SMB of the AIS is determined for 90 % by snowfall and (ii) the good agreement in T_{2m} and snowfall increase (following the Clausius Clapeyron relation), results in a ΔT_{2m}-ΔSMB relation with good spatial and temporal agreement. In R-H3-A1B, these relations are valid for a temperature range of at least $\sim$6 K, which is three times larger than the differences between the historical simulations (R-ERA, R-H3 and R-E5). Therefore it is reasonable to assume that the results presented here are representative for a future temperature rise of at least 4 K. Also beyond this temperature increase it is likely that the T_{2m}-SMB relation remains valid, because runoff remains only locally important during our simulations and the other mass removing SMB-component, sublimation, is rather constant and not expected to strongly increase in a warming climate.

Acknowledgments We thank two anonymous reviewers and Peter Kuipers Munneke for their extensive and valuable comments, which definitely helped to improve the quality and structure of the paper. We acknowledge the Netherlands Polar Program of NWO/ALW and the ice2sea project, funded by the European Commissions 7th Framework Programme through grant number 226375, ice2sea manuscript number 085.

References

Bengtsson L, Koumoutsaris S, Hodges K (2011) Large-scale surface mass balance of ice sheets from a comprehensive atmospheric model. Surv Geophys 32:459–474. doi:10.1007/s10712-011-9120-8

Chapman WL, Walsh JE (2007) Simulations of Arctic temperature and pressure by Global Coupled Models. J Clim 20:609–632. doi:10.1175/JCLI4026.1

Church JA et al (2011) Revisiting the Earth's sea-level and energy budgets from 1961 to 2008. Geophys Res Lett 38(L18601). doi:10.1029/2011GL048794

Connolley WM, Bracegirdle TJ (2007), An Antarctic assessment of IPCC AR4 coupled models. Geophys Res Lett 34(L22505). doi:10.1029/2007GL031648

Davis CH, Li Y, McConnell JR, Frey MM, Hanna E (2005) Snowfall-driven growth in East Antarctic ice sheet mitigates recent sea-level rise. Science 308:1898–1901. doi:10.1126/science.1110662

Dee DP et al (2011) The ERA-Interim reanalysis: configuration and performance of the data assimilation system. Q J R Meteorol Soc 137(656):553–597. doi:10.1002/qj.828

Ettema J (2010) The present-day climate of Greenland: a study with a regional climate model. PhD thesis, Utrecht University, pp 123, (http://igitur-archive.library.uu.nl/dissertations/2010-0408-200308/uuindex.html).

Ettema J, van den Broeke MR, van Meijgaard E, van de Berg WJ, Bamber J, Box JE, Bales RC (2009) Higher surface mass balance of the Greenland ice sheet revealed by high-resolution climate modeling. Geophys Res Lett 36(L12501). doi:10.1029/2009GL038110

Franco B, Fettweis X, Erpicum M, Nicolay S (2011) Present and future climates of the Greenland ice sheet according to the IPCC AR4 models. Clim Dyn 36:1897–1918. doi:10.1007/s00382-010-0779-1

Gordon C, Cooper C, Senior CA, Banks H, Gregory JM, Johns TC, Mitchell JFB, Wood RA (2000) The simulation of SST, sea ice extents and ocean heat transports in a version of the Hadley Centre coupled model without flux adjustments. Clim Dyn 16:147–168. doi:10.1007/s003820050010

Gregory JM, Huybrechts P (2006) Ice-sheet contributions to future sea-level change. Philos Trans R Soc A 364:1709–1731. doi:10.1098/rsta.2006.1796

Held IM, Soden BJ (2006) Robust response of the hydrological cycle to global warming. J Clim 19:5686–5699. doi:10.1175/JCLI3990.1

Hellmer HH, Kauker F, Timmermann R, Determann J, Rae J (2012) Twenty-first-century warming of a large Antarctic ice-shelf cavity by a redirected coastal current. Nature 485:225–228. doi:10.1038/nature11064

IPCC (2007) Climate Change 2007: The physical science basis. Contribution of working group I to the fourth assessment report of the intergovernmental panel on climate change. Cambridge University Press, Cambridge, pp 996

Johns TC et al (2011), Climate change under aggressive mitigation: the ENSEMBLES multi-model experiment. Clim Dyn 37:1975–2003. doi:10.1007/s00382-011-1005-5

Krinner G, Magand O, Simmonds I, Genthon C, Dufresne J-L (2007) Simulated Antarctic precipitation and surface mass balance at the end of the twentieth and twenty-first centuries. Clim Dyn 28:215–230. doi:10.1007/s00382-006-0177-x

Kuipers Munneke P, van den Broeke MR, Lenaerts JTM, Flanner MG, Gardner AS, van de Berg WJ (2011) A new albedo parameterization for use in climate models over the Antarctic ice sheet. J Geophys Res 116(D05114). doi:10.1029/2010JD015113

Lenaerts JTM, Van den Broeke MR (2012) Modeling drifting snow in Antarctica with a regional climate model, part II: results. J Geophys Res 117(D05109). doi:10.1029/2010JD015419

Lenaerts JTM, van den Broeke MR, van de Berg WJ, van Meijgaard E, Kuipers Munneke P (2012a) A new, high-resolution surface mass balance map of Antarctica (1979–2010) based on regional atmospheric climate modeling. Geophys Res Lett 39(L04501). doi:10.1029/2011GL050713

Lenaerts JTM, van den Broeke MR, Scarchilli C, Agosta C (2012b) Impact of model resolution on simulated wind, drifting snow and surface mass balance in Terre Adélie, East Antarctica. J Glaciol 58(211):821–829. doi:10.3189/2012JoG12J020

Levermann A et al (2012) Projecting Antarctic ice discharge using response functions from SeaRISE ice-sheet models. Cryosphere Discuss. 6:3447–3489. doi:10.5194/tcd-6-3447-2012

Lowe JA, Hewitt CD, van Vuuren DP, Jones TC, Stehfest E, Royer J-F, van der Linden PJ (2009) New study for climate modeling, analyses, and scenarios. EOS Trans AGU 90(21):181. doi:10.1029/2009EO210001

Lythe MB, Vaughan DG, the BEDMAP Consortium (2001) BEDMAP: a new ice thickness and subglacial topographic model of Antarctica. J Geophys Res 106(B6):11335–11352. doi:10.1029/2000JB900449

Maris MNA, de Boer B, Oerlemans J (2012) A model comparison study for the Antarctic region: present and past. Clim Past 8:803–814. doi:10.5194/cp-8-803-2012

Monaghan AJ, Bromwich DH, Chapman W, Comiso JC (2008) Recent variability and trends of Antarctic near-surface temperature. J Geophys Res 113(D04105). doi:10.1029/2007JD009094

Muller WA, Roeckner E (2007) ENSO teleconnections in projections of future climate in ECHAM5/MPI-OM. Clim Dyn 31:533–549. doi:10.1007/s00382-007-0357-3

Nakicenovic N et al (2000) IPCC special report on emissions scenarios (SRES). Cambridge University Press, Cambridge

Nicholls RJ, Cazenave A (2010) Sea-level rise and its impact on coastal zones. Science 328(1517). doi:10.1126/science.1185782

Picard G, Domine F, Krinner G, Arnaud L, Lefebvre E (2012) Inhibition of the positive snow-albedo feedback by precipitation in interior Antarctica. Nat Clim Change 2:795–798. doi:10.1038/nclimate1590

Pope VD, Pamment JA, Jackson DR, Slingo A (2000) The representation of water vapor and its dependence on vertical resolution in the Hadley Centre climate model. J Clim 14:3065–3085. doi:10.1175/1520-0442(2001)014<3065:TROWVA>2.0.CO;2

Pritchard HD, Arthern RJ, Vaughan DG, Edwards LA (2009) Extensive dynamic thinning on the margins of the Greenland and Antarctic ice sheets. Nature 461:971–975. doi:10.1038/nature08471

Pritchard HD, Ligtenberg SRM, Fricker HA, Vaughan DG, van den Broeke MR, Padman L (2012) Antarctic ice-sheet loss driven by basal melting of ice shelves. Nature 484:502–505. doi:10.1038/nature10968

Rignot E, Jacobs SS (2002) Rapid bottom melting widespread near Antarctic ice sheet grounding lines. Science 296(2020), doi:10.1126/science.1070942

Rignot E, Bamber JL, van den Broeke MR, Davis C, Li Y, van de Berg WJ, van Meijgaard E (2008) Recent Antarctic ice mass loss

from radar interferometry and regional climate modelling. Nature Geosci 1:106–110. doi:10.1038/ngeo102

Rignot E, Velicogna I, van den Broeke MR, Monaghan A, Lenaerts JTM (2011) Acceleration of the contribution of the Greenland and Antarctic ice sheets to sea level rise. Geophys Res Lett 38(L05503). doi:10.1029/2011GL046583

Sheperd A, Ivins ER, Geruo A, IMBIE project group (2012) A reconciled estimate of ice-sheet mass balance. Science 338:1183–1189. doi:10.1126/science.1228102

Uppala SM et al (2005) The ERA-40 re-analysis. Q J R Meteorol Soc 131(612):2961–3012. doi:10.1256/qj.04.176

Van de Berg WJ, van den Broeke MR, Reijmer CH, van Meijgaard E (2006) Reassessment of the Antarctic surface mass balance using calibrated output of a regional atmospheric climate model. J Geophys Res 111(D11104). doi:10.1029/2005JD006495

Van den Broeke MR (2008) Depth and density of the Antarctic firn layer. Arct Antarct Alp Res 40(2):432–438. doi:10.1657/1523-0430(07-021)[BROEKE]2.0CO;2

Van den Broeke MR, Van Lipzig NPM (2004) Changes in Antarctic temperature, wind and precipitation in response to the Antarctic Oscillation. Ann Glaciol 39:119–126. doi:10.3189/172756404781814654

Van den Broeke MR, Bamber J, Lenaerts J, Rignot E (2011) Ice sheets and sea level: thinking outside the box. Surv Geophys. doi:10.1007/s10712-011-9137-z

Van Lipzig NPM, van Meijgaard E, Oerlemans J (2002) Temperature sensitivity of the Antarctic surface mass balance in a regional atmospheric climate model. J Clim 15:2758–2774. doi:10.1175/1520-0442(2002)015<2758:TSOTAS>2.0.CO;2

Van Meijgaard E, van Ulft LH, van de Berg WJ, Bosveld FC, van den Hurk BJJM, Lenderink G, Siebesma AP (2008) The KNMI regional atmospheric climate odel RACMO version 2.1. Royal Netherlands Meteorological Institute De Bilt, The Netherlands

Velicogna I (2009) Increasing rates of ice mass loss from the Greenland and Antarctic ice sheets revealed by GRACE. Geophys Res Lett 36(L19503). doi:10.1029/2009GL040222

Wild M, Calanca P, Scherrer SC, Ohmura A (2003) Effects of polar ice sheets on global sea level in high-resolution greenhouse scenarios, J Geophys Res 108(D5):4165. doi:10.1029/2002JD002451